Structures with Multiple Equilibrium Configurations due to Prestress and Unilateral Contacts

Charles Dorn
Graduate Aerospace Laboratories
California Institute of Technology
Pasadena, California 91125, USA
Email: cdorn@caltech.edu

Yang Li
The Institute of Technological Sciences
Wuhan University
Wuhan, Hubei 430072, PR China
Email: yang.li@whu.edu.cn

Sergio Pellegrino
Graduate Aerospace Laboratories
California Institute of Technology
Pasadena, California 91125, USA
Email: sergiop@caltech.edu

This paper presents structures with multiple equilibrium configurations arising from the combination of a state of prestress and unilateral contacts. A design problem is posed where preloaded elastic springs and unilateral constraints are embedded throughout a mechanism. The spring parameters are designed such that multiple target configurations are immobilized due to contact. In each of these configurations, the spring forces maintain compressive reaction forces, immobilizing the structure. Each immobilized configuration can rigidly resist perturbation forces up to some finite magnitude where contact is lost. Hence, this case of multiple configurations in equilibrium due to the combination of prestress and contact is referred to as multi-configuration rigidity. Two examples of structures exhibiting multi-configuration rigidity are presented. First, a four bar linkage with a single kinematic degree of freedom is used to introduce the concept. In the context of the linkage, multi-configuration rigidity is compared to multi-stability, exhibiting the key differences between the two concepts. Then, a 24-degree-of-freedom kirigami surface is presented that can morph between flat and spherical configurations, motivated by RF antenna applications. By embedding torsional springs and fold angle stops throughout the structure, the flat and spherical configurations are made rigid. Actuation between the configurations can easily be achieved by snapping the structure between the rigid configurations.

1 Introduction

This study defines and explores the concept of multi-configuration structural rigidity, based on embedding unilateral stops and springs in a structure with one or more internal mechanisms that allow the structure to take up multiple specified target configurations. In each of these configurations, the structure is held rigidly by the springs maintaining contact with the unilateral stops. It is shown that multi-configuration rigidity is a useful concept in the design of reconfigurable structures.

Multi-configuration rigidity is particularly useful in the context of origami structures with many internal mechanisms, defined as the degrees of freedom (DOFs) of the structure. Practical application of origami is often limited to patterns with single or low-DOF since they can be easily actuated. However, the geometry of low-DOF structures is inherently limited by their low dimensional configuration space. In contrast, many-DOF patterns such as Resch's pattern [1] have more geometric freedom and can exhibit remarkable geometric changes [2].

Many-DOF structures are alluring for engineering applications due to their geometric versatility, but actuation can be prohibitively complex [3]. The "brute force" actuation strategy of simultaneously controlling a number of actuators equal to the DOFs of the structure [4] is impractical to physically implement. Active materials show promise for actuating many-DOF patterns, which might utilize thermal or electrical stimuli to locally activate folding [5–8], but are suited for smaller scale applications without significant load-bearing capabilities. Another approach for reconfiguring many-DOF structures is through multi-stability, as proposed in [9]. Springs are embedded throughout a structural mechanism, and the spring parameters are designed such that each target configuration corresponds to a stable equilibrium configuration. The actuation of a multi-stable structure is straightforward since transferring between stable configurations can easily be achieved.

Multi-configuration rigidity is different from multi-

stability. Whereas multi-stable structures have analytical (smooth) energy minima at each stable configuration, in multi-configuration rigidity the kinematic boundary introduced by the unilateral constraints introduces a sharp local energy minimum for each rigid configuration. Multi-configuration rigidity offers key advantages compared to multi-stability, such as the ability to resist finite perturbation loads without significant deflection (theoretically, zero deflection).

The idea of utilizing unilateral constraints to aid in structural reconfigurations has been previously considered to control shape changes in many-DOF metamaterials [10]. Contact has been used to simplify reconfiguration of a linkage [11] and also rigidity of structures due to contact is found in bio-inspired structures such as scales [12]. Furthermore, insightful parallels can be drawn to concepts in the robotic grasping literature [13] [14], which shows examples of immobilizing objects using unilateral contacts.

This paper provides examples of the design of structures that have multiple rigid configurations. Two structures are studied: a single-DOF linkage and a 24-DOF kirigami surface. The conditions for rigidity are derived for each structure and a set of springs is designed to achieve rigidity in specified configurations. A prototype of the 24-DOF kirigami surface is constructed using lamina emergent torsional hinges [15] to act as torsional springs. The applicability of multi-configuration rigidity to practical engineering structures is demonstrated by fitting a prototype of the kirigami surface with RF antennas to create a morphing phased array [16].

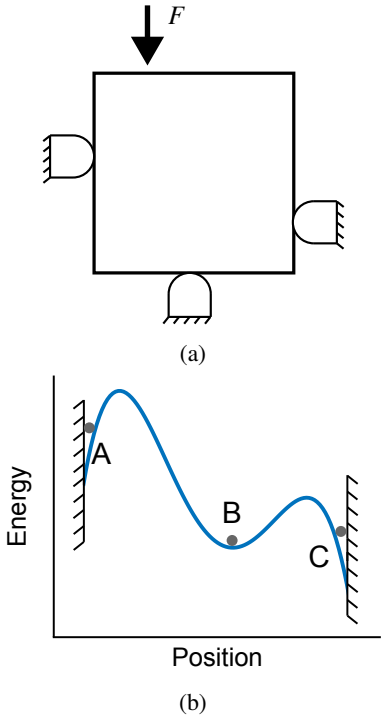

Fig. 1: Interpretations of rigidity due to unilateral constraints. (a) Object grasping analogy. The square is in *force closure*, immobilized due to contact with unilateral constraints, which is maintained due to the force F. (b) Ball on a hill analogy. Points A and C are held rigidly due to contact with the wall, while Point B is a stable equilibrium position.

2 Interpretations of multi-configuration rigidity

Two interpretations of multi-configuration rigidity are provided by a robotic grasping analogy and by considering a ball moving on a hill, in two dimensions. These interpretations are generalized to higher dimension in Section 4 in the context of a 24-DOF structure.

The first interpretation considers a robotic grasping problem, which is useful in understanding how a single configuration is immobilized by contact. Figure 1a shows an object grasped by three frictionless unilateral constraints. Since the force F is present and pushes into the constraints, contact with the constraints is maintained and the object is immobilized. This is referred to as *force closure* in the grasping literature [13]. Force closure occurs when an external force acts to maintain contact with unilateral constraints to immobilize an object (note that the precise definition of force closure varies in the literature [14] [17]). When subjected to a perturbing force, the object will not move unless the perturbing force has an upward vertical component larger than F, and is thus rigid up to some finite perturbation. This grasping analogy offers a useful interpretation of structural rigidity from unilateral constraints, where F is analogous to the force in the springs, which pushes against the unilateral constraints to block any possible motion.

A second interpretation is the classical "ball on a hill" analogy, shown in Figure 1b, where the walls represent the unilateral constraints. Points A and C are local minima with respect to kinematically admissible positions that respect the unilateral constraints, corresponding to the hill sloping into the wall. If a perturbation force is applied to the ball, it will not move unless the weight of the ball is overcome by the force. Thus, points A and C identify two rigid configurations. In contrast, point B is a smooth local energy minimum, which corresponds to a stable equilibrium configuration.

3 Single-DOF example

This section presents a simple single-DOF linkage that is designed to achieve rigidity in two target configurations. Consider the four-bar linkage shown in Figure 2 with bar lengths $AB = 0.8$, $BC = 1.16$, $CD = 1.3$, and $AD = 0.95$. This linkage itself represents the *skeleton* structure, which is kinematically indeterminate with one degree of freedom. The kinematics can be described in terms of a single variable, which will be taken as θ_A. An analytical relation between θ_D and θ_A is given by [18]

$$\theta_D = \pi - \arctan\left(\frac{A_2}{A_1}\right) \pm \arccos\left(\frac{-A_3}{\sqrt{A_1^2 + A_2^2}}\right), \quad (1)$$

where

$$A_1 = 2AB \cdot CD\cos\theta_A - 2AD \cdot CD \tag{2}$$
$$A_2 = 2AB \cdot CD\sin\theta_A \tag{3}$$
$$A_3 = AD^2 + CD^2 + AB^2 - BC^2 - 2AB \cdot AD\cos\theta_A. \tag{4}$$

The kinematic path in the space of θ_A and θ_D is plotted in Figures 3a and 4a.

The two configurations shown in Figure 2 are taken as target configurations. The first target configuration has angles $\theta_A = -191^\circ$ and $\theta_D = 90^\circ$ while the second has $\theta_A = 83^\circ$ and $\theta_D = 90^\circ$. Linear torsional springs of stiffness k are introduced on joints A and D. The energy stored in the springs is

$$E = \frac{1}{2}k\left(\theta_A - \theta_A^0\right)^2 + \frac{1}{2}k\left(\theta_D - \theta_D^0\right)^2, \tag{5}$$

where θ_A^0 and θ_D^0 are the rest angles of the two springs. The rest angles of the springs constitute the two design variables in the problem, which can be designed to make the structure have two rigid (Section 3.1) or stable (Section 3.2) configurations. Since the stiffnesses of the springs are equal, the actual value does not affect the shape of the energy landscape and only acts as a scaling factor.

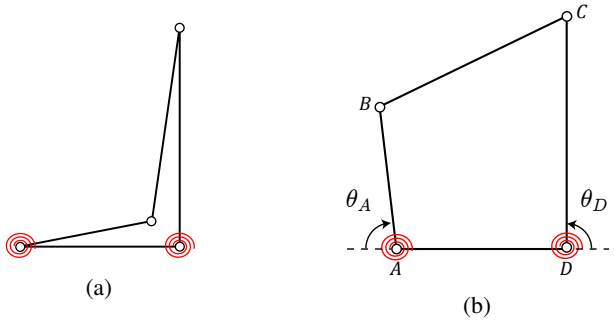

(a) (b)

Fig. 2: Four bar linkage geometry with torsion springs on A and D (red). (a) Target configuration 1 with $\theta_A = -191^\circ$ and $\theta_D = 90^\circ$. (b) Target configuration 2 with $\theta_A = 83^\circ$ and $\theta_D = 90^\circ$.

3.1 Multi-configuration rigidity

To achieve multi-configuration rigidity, we introduce a unilateral constraint to restrict the angle θ_D to

$$\theta_D \geq 90^\circ. \tag{6}$$

Note that this constraint is *active* ($\theta_D = 90^\circ$) in both target configurations. That is, both configurations lie on the boundary of the kinematically admissible configurations. Associated with this unilateral constraint is a reaction moment μ.

The problem at hand is to design the rest angles of the torsional springs such that both target configurations are rigid due to contact with the 90° stop. Specifically, the rest angles should be designed such that the reaction moment μ in the angle stop on θ_D is positive in both configurations.

The equilibrium conditions in the presence of constraints can be written by introducing a Lagrange multiplier. The *Lagrangian function* is defined as

$$\mathcal{L} = E + \mu(90^\circ - \theta_D), \tag{7}$$

where the Lagrange multiplier μ represents the reaction moment of the unilateral constraint. The equilibrium conditions are

$$\frac{\partial \mathcal{L}}{\partial \theta_A} = \frac{dE}{d\theta_A} - \mu\frac{d\theta_D}{d\theta_A} = 0 \tag{8}$$
$$\mu \geq 0 \tag{9}$$
$$\mu(\theta_D - 90^\circ) = 0, \tag{10}$$

which are known as the Karush-Kuhn-Tucker conditions [19]. Equation (8) represents a generalized force balance and (9) enforces the condition that the contact moment in the unilateral constraint must be non-negative. Finally, Eq. (10) requires that μ can only be nonzero if there is contact with the constraint, known as the complementarity condition.

Examining Eq. (10), if $\mu > 0$ then θ_D must remain equal to 90° and the structure is rigid. To achieve multi-configuration rigidity, we seek values of θ_A^0 and θ_D^0 that correspond to positive μ's in both target configurations.

Solving for μ in Eq. (8) and requiring its positivity yields

$$\mu = \frac{dE}{d\theta_A}\left(\frac{d\theta_D}{d\theta_A}\right)^{-1} \tag{11}$$
$$= k\left(\theta_A - \theta_A^0 + \left(\theta_D - \theta_D^0\right)\frac{d\theta_D}{d\theta_A}\right)\left(\frac{d\theta_D}{d\theta_A}\right)^{-1} > 0. \tag{12}$$

Enforcing $\mu > 0$ in both target configurations leads to a system of two inequalities restricting θ_A^0 and θ_D^0. The solution to this system is the blue shaded region in Figure 3a. Designing the rest angle in this region leads to rigidity in both target configurations.

The energy profile along the kinematic path corresponding to $\theta_A = 0$ and $\theta_D = -180^\circ$, a design in the blue shaded region of Fig. 3a, is plotted in Figure 3b. Each target configuration is a sharp energy minimum, lying on the boundary of the kinematically admissible domain.

An alternative approach to the rigidity of this linkage is obtained by considering a perturbing moment acting on the structure. A rigid configuration can resist perturbing moments without any displacement, up to some finite value of

the perturbation when contact is lost. Consider, for example, a counterclockwise perturbation moment $\tilde{M}_A$ applied at point A in target configuration 1. The generalized force balance accounting for the perturbing moment becomes:

$$\frac{dE}{d\theta_A} - \tilde{\mu}\frac{d\theta_D}{d\theta_A} - \tilde{M}_A = 0, \tag{13}$$

where $\tilde{\mu}$ is the reaction moment after the perturbing moment is applied. Solving for $\tilde{\mu}$ gives

$$\tilde{\mu} = \left(\frac{dE}{d\theta_A} - \tilde{M}_A\right)\left(\frac{d\theta_D}{d\theta_A}\right)^{-1} = \mu - \tilde{M}_A\left(\frac{d\theta_D}{d\theta_A}\right)^{-1}. \tag{14}$$

Here, μ is the reaction force in the absence of the perturbation from Eq. (11).

Assuming that the rest angles fall within the blue region of Figure 3a, μ is positive. Therefore, since $\frac{d\theta_D}{d\theta_A}$ is positive in configuration 1, as long as $\tilde{M}_A < \mu\frac{d\theta_D}{d\theta_A}$, then $\tilde{\mu}$ is positive and θ_D must remain at 90°. In other words, the structure can rigidly resist perturbation moments up to a finite magnitude.

3.2 Distinction from multi-stability

It is important to distinguish between multi-configuration rigidity and multi-stability. While they are similar in some regards, multi-configuration rigidity has key advantages when compared to multi-stability, which can be exemplified by studying the 4-bar linkage.

We aim to compute the rest angles that lead to bi-stability in target configurations 1 and 2. At each target configuration, with respect to θ_A the first derivative of the energy must be zero (equilibrium) and the second derivative must be positive (stability):

$$\frac{dE}{d\theta_A} = k\left(\theta_A - \theta_A^0\right) + k\left(\theta_D - \theta_D^0\right)\frac{d\theta_D}{d\theta_A} = 0 \tag{15}$$

$$\frac{d^2E}{d\theta_A^2} = k\left(1 + \frac{d\theta_D}{d\theta_A}^2\right) + k\left(\theta_D - \theta_D^0\right)\frac{d^2\theta_D}{d\theta_A^2} > 0. \tag{16}$$

Enforcing equations Eqs. (15) and (16) at both target configurations, there is a unique solution for the rest angles of $\theta_A^0 = 45.9°$ and $\theta_D^0 = 32.2°$. Figure 4a shows the rest angle solution that leads to bi-stability. The energy along the kinematic path is shown in Figure 4b, where it is clear that both target configurations are smooth energy minima, in contrast to the boundary minima in the previous section.

By comparing the rigid and stable examples, two advantages of multi-configuration rigidity are observed. First, a large set of allowable rest angles leads to rigidity compared to a unique solution in the bi-stability case. This is because bi-stability requires an equation (Eq. (15)) and an inequality (Eq. (16)) to be satisfied at each target configuration. However, the rigidity conditions are less strict, only requiring a single inequality (Eq. (12)) to hold in each configuration. In practice, it is useful to have a set of allowable designs, since a precise value of stiffness and rest angle cannot be exactly achieved. The second advantage of multi-configuration rigidity is the ability to resist loads (below some critical value when contact is lost) without any displacement. Thus, at least theoretically, there is an infinite initial stiffness with respect to perturbation forces. In contrast, for multi-stability the structure will deform elastically in response to any perturbation and, often, the energy minima have low stiffness.

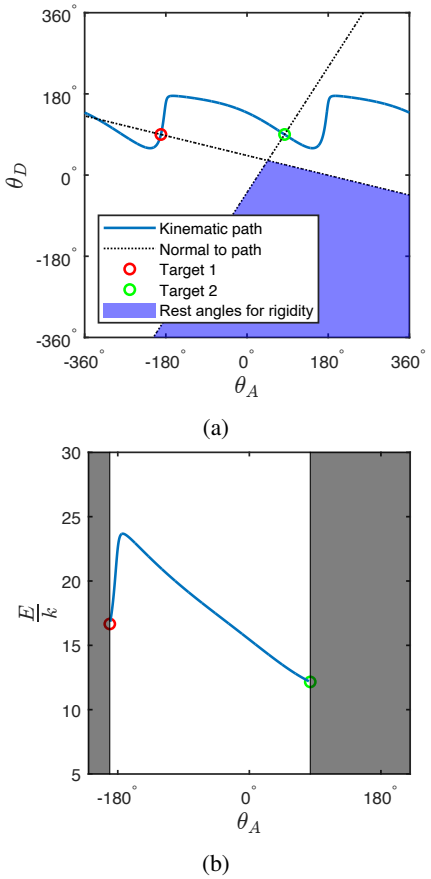

Fig. 3: Four bar linkage solution for rigidity at both target configurations. (a) Plot of the kinematic path and rest angles that lead to multi-configuration rigidity, in $\theta_A\theta_D$-space. (b) Energy profile along the kinematic path corresponding to $\theta_A^0 = 0$ and $\theta_D^0 = -180°$, which is a design in the blue region of (a). The dark shaded regions violate $\theta_D \geq 90°$.

4 A 24-DOF surface with two rigid configurations

To demonstrate multi-configuration rigidity in a complex structure, an example is presented of a 24-DOF kirigami pattern that can morph between a spherical configuration and a flat configuration. A set of angle stops are added throughout the structure to restrict the fold angles. Torsional springs are embedded along every fold of the structure, and the stiffness and rest angles of these springs are designed such that both the flat and spherical configurations satisfy the conditions for rigidity. The usefulness of multi-

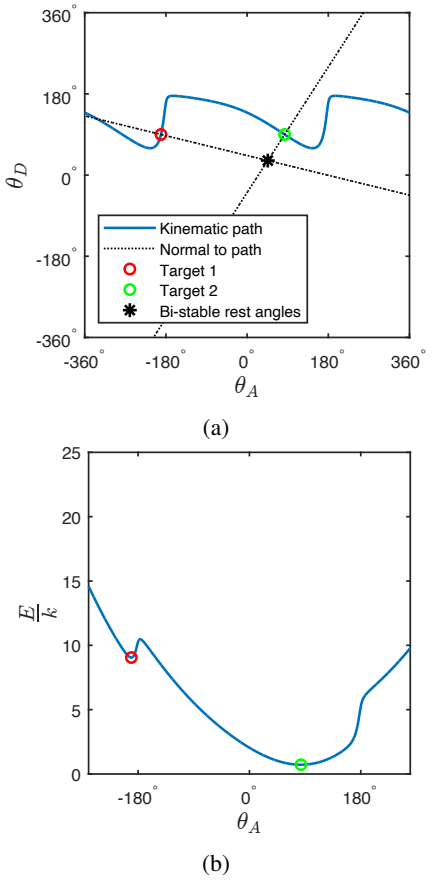

Fig. 4: Four bar linkage solution for bi-stablity. (a) Plot of the kinematic path and rest angles that lead to bi-stability, in $\theta_A\theta_D$-space. (b) Energy profile along the kinematic path for the bi-stable design $\theta_A^0 = 45.9°$ and $\theta_D^0 = 32.2°$.

configuration rigidity for practical engineering applications is demonstrated by constructing a prototype of the morphing surface that is outfitted with antennas to create a functional morphing phased-array antenna.

4.1 Geometry

Figure 5 shows the geometry of the morphing surface. The geometry consists of a set of square tiles, shown in green, that are connected by trapezoidal folds, shown in gray. The pattern can morph between flat and spherical surfaces, where the tiles lie on a sphere in the spherical configuration and are co-planar in the flat configuration. The pattern itself is non-developable, so it cannot be entirely flattened such that all faces (both green and gray) become co-planar.

Synthesis of this fold pattern follows a two-step process. First, the tiles are arranged on the surface of a sphere, shown in Figure 5a. The tile arrangement problem is formulated as a constrained optimization problem and is presented in detail in [20]. In this study a sphere with a radius of 2.9 times the tile edge length is considered. The second step in the geometry synthesis process connects the adjacent tiles with valley folds, shown in gray in Figure 5b. The gray faces are added perpendicular to the tiles so all mountain folds are at 90° in the spherical configuration. Finally, upon closing the valley folds a flat configuration is achieved where the tiles come together to make a planar square grid, shown in Figure 5c.

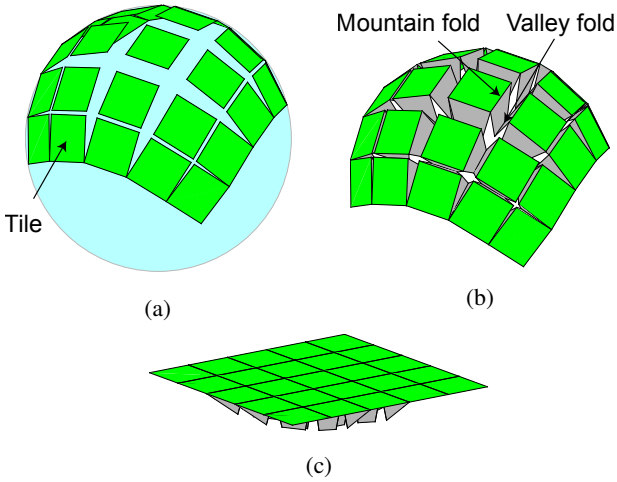

Fig. 5: Geometry of the morphing surface kirigami pattern. (a) Arrangement of tiles on a sphere. (b) Valley folds are inserted perpendicular to the tiles to connect adjacent tiles, resulting in the spherical configuration. (c) Upon closing the valley folds, the flat configuration is achieved.

In the flat configuration, the mountain folds are at 90° and the valley folds are at 180°. In the spherical configuration, the mountain folds are at 90°, while the valley folds take on a range of angles between 150° and 160°.

4.2 Kinematics

This section defines a set of bilateral and unilateral constraints that capture the kinematics of the structure.

The geometry of the structure is defined by vertex coordinates $\boldsymbol{x} \in \mathbb{R}^{3n}$ where n is the number of vertices in the structure. Denote $\boldsymbol{\theta}_m \in \mathbb{R}^{n_m}$ and $\boldsymbol{\theta}_v \in \mathbb{R}^{n_v}$ as vectors containing the angles of the n_m mountain folds and n_v valley folds, respectively.

A network of rigid bars and fixed hinges can be used to capture the plate-hinge kinematics [21]. Each edge in the pattern is replaced with a rigid bar of fixed length. Then, each quadrilateral face in the pattern is triangulated by adding a rigid bar across a diagonal. Planarity of the quadrilateral faces is enforced by constraining the angle φ about the added bar on the diagonal to be zero. Overall, the bilateral constraints $\boldsymbol{h}(\boldsymbol{x})$ corresponding to the n_b rigid bars and n_h fixed hinges takes the form:

$$\boldsymbol{h}(\boldsymbol{x}) = \boldsymbol{0}, \tag{17}$$

where

$$h_i(\boldsymbol{x}) = \begin{cases} l_i(\boldsymbol{x}) - L_i & i = 1,...,n_b \\ \varphi_i(\boldsymbol{x}) & i = n_b+1,...,n_b+n_h. \end{cases} \tag{18}$$

Here, $l_i(\boldsymbol{x})$ is the length of bar i in configuration $\boldsymbol{x}$, which is fixed at length L_i, and $\varphi_i(\boldsymbol{x})$ is the angle of a triangulating hinge, which is fixed at 0. For a more in-depth discussion of this kinematic model, see [9].

The bilateral constraint gradients $\boldsymbol{C}^b \in \mathbb{R}^{(n_b+n_h)\times 3n}$, which form the compatibility matrix of the bilateral constraints, are defined as

$$\boldsymbol{C}^b = \frac{\partial \boldsymbol{h}}{\partial \boldsymbol{x}} = \begin{bmatrix} \dfrac{\partial \boldsymbol{l}}{\partial \boldsymbol{x}} \\ \dfrac{\partial \boldsymbol{\varphi}}{\partial \boldsymbol{x}} \end{bmatrix}. \tag{19}$$

The gradients of bar lengths and hinge rotations with respect to $\boldsymbol{x}$, which make up $\boldsymbol{C}^b$, are derived in [9].

The linearized bilateral constraints take the form

$$\boldsymbol{C}^b \boldsymbol{d} = \boldsymbol{0}, \tag{20}$$

where $\boldsymbol{d} \in \mathbb{R}^{3n}$ is a displacement of the vertices.

A first-order compatible displacement $\boldsymbol{d}_m$ must lie within the m-dimensional null space of $\boldsymbol{C}^b$, where m is the number of kinematic degrees of freedom of the structure, and was previously denoted as DOF. For the kirigami surface $m = 24$.

Along with the bilateral constraints, unilateral constraints are considered in the form of restrictions on the fold angles, which are introduced to achieve multi-configuration rigidity. Observing that both the flat and spherical configurations have 90° mountain fold angles, we choose to restrict the mountain fold angles to be greater than 90°. The unilateral constraints take the form

$$90^\circ - \theta_{mj}(\boldsymbol{x}) \leq 0, \quad j = 1,...,n_m. \tag{21}$$

The gradients of the unilateral constraint functions are defined as $\boldsymbol{C}^u \in \mathbb{R}^{n_m \times 3n}$, where

$$\boldsymbol{C}^u = -\frac{\partial \boldsymbol{\theta}_m}{\partial \boldsymbol{x}}. \tag{22}$$

More details about the angle gradients are provided in [9].

4.3 Equilibrium

Linear torsional springs are introduced on each fold of the structure. To simplify the problem, it is assumed that all springs on the mountain folds are identical and all springs on the valley folds are identical. Hence, the energy stored in the springs takes the form

$$E = \sum_{i=1}^{n_m} \frac{1}{2} k_m (\theta_{mi} - \theta_m^0)^2 + \sum_{i=1}^{n_v} \frac{1}{2} k_v (\theta_{vi} - \theta_v^0)^2, \tag{23}$$

where k_m and θ_m^0 are the stiffness and rest angle of the mountain folds and k_v and θ_v^0 are the stiffness and rest angle of the valley folds. The spring parameters are design variables, which will be chosen to achieve rigidity in both the spherical and flat configurations. Since scaling of the energy does not affect the shape of the energy landscape, only three design variables must be considered: k_v/k_m, θ_m^0, and θ_v^0.

Now that a set of springs has been introduced, the equilibrium conditions can be derived from the Lagrangian function

$$\mathcal{L} = E + \boldsymbol{\mu}^T (90^\circ - \boldsymbol{\theta}_m) + \boldsymbol{\lambda}^T \boldsymbol{h}(\boldsymbol{x}), \tag{24}$$

where $\boldsymbol{\mu} \in \mathbb{R}^{n_m}$ are the reactions of the unilateral constraints on the mountain folds and $\boldsymbol{\lambda} \in \mathbb{R}^{n_b+n_h}$ are the reactions of the bilateral constraints. The constraint reactions are generalized forces, which for angle constraints correspond to reaction moments and for rigid bar constraints correspond to bar forces.

The equilibrium conditions, which take the form of the Karush-Kuhn-Tucker conditions, are

$$\frac{\partial \mathcal{L}}{\partial \boldsymbol{x}} = \frac{dE}{d\boldsymbol{x}} + \boldsymbol{\mu}^T \boldsymbol{C}^u + \boldsymbol{\lambda}^T \boldsymbol{C}^b = 0 \tag{25}$$

$$\mu_i \geq 0, \quad i = 1,...,n_m \tag{26}$$

$$\mu_i(\theta_{mi} - 90^\circ) = 0, \quad i = 1,...,n_m. \tag{27}$$

Equation (25) represents a generalized force balance, while Eq. (26) requires the unilateral constraint reactions to be non-negative. Equation (27) states that a unilateral reaction can only be nonzero if there is contact with the constraint.

Given a set of spring parameters, which determines $\frac{\partial E}{\partial \boldsymbol{x}}$, the constraint reaction forces can be computed. Equation (25) is a linear system with respect to $\boldsymbol{\mu}$ and $\boldsymbol{\lambda}$, which can be written as

$$\begin{bmatrix} \boldsymbol{C}^{uT} & \boldsymbol{C}^{bT} \end{bmatrix} \begin{bmatrix} \boldsymbol{\mu} \\ \boldsymbol{\lambda} \end{bmatrix} = -\frac{\partial E}{\partial \boldsymbol{x}}. \tag{28}$$

If Eq. (28) has no solution where all components of $\boldsymbol{\mu}$ are non-negative, then equilibrium is violated. If a solution exists, the reactions will not be unique if the structure is statically indeterminate, which is the case for the kirigami surface. Although the equilibrium solution is non-unique, the value of any perturbation force at which the structure loses its rigidity is unique.

4.4 Designing for rigidity

A design problem is posed to select spring parameters k_v/k_m, θ_m^0, and θ_v^0 such that both the flat and spherical configurations are both rigid. Rigidity occurs when positive unilateral reactions $\boldsymbol{\mu}$ satisfy equilibrium, since there are $n_u = 80$ unilateral constraints (stops on the 80 mountain folds), which are enough to block motion along the $m = 24$ mechanisms. The design space is is limited to only three variables, allowing for a direct search of the design space to evaluate which designs lead to rigidity.

A search was performed in the region $-360^\circ \leq \theta_m^0 \leq 360^\circ$, $-360^\circ \leq \theta_v^0 \leq 360^\circ$, $0.1 \leq k_v, k_m \leq 10$. At any given point in this region, the solution to Eq. (28) can be evaluated in both configurations to check for positive unilateral reactions. By evaluating many designs, the design space can be partitioned into regions where the rigidity condition is satisfied for each configuration.

Figure 6 shows the regions of the design space where rigidity is achieved in the spherical and flat configurations. The axes of these plots correspond to the rest angles of the mountain and valley folds. In the black regions, equilibrium is violated for all values of the valley to mountain stiffness ratio, k_v/k_m. In the white regions, the rigidity conditions are satisfied for some or all values of k_v/k_m.

The design chosen for building the prototype in the next section has $\theta_v^0 = 180^\circ$ and $\theta_m^0 = 0^\circ$, and corresponds to the red dot in Figure 6. For these rest angles, as long as $k_v/k_m < 1.33$, the structure satisfies the rigidity conditions in both the spherical and flat configurations. These rest angles are desirable since they not only satisfy the rigidity conditions, but they are straightforward to fabricate.

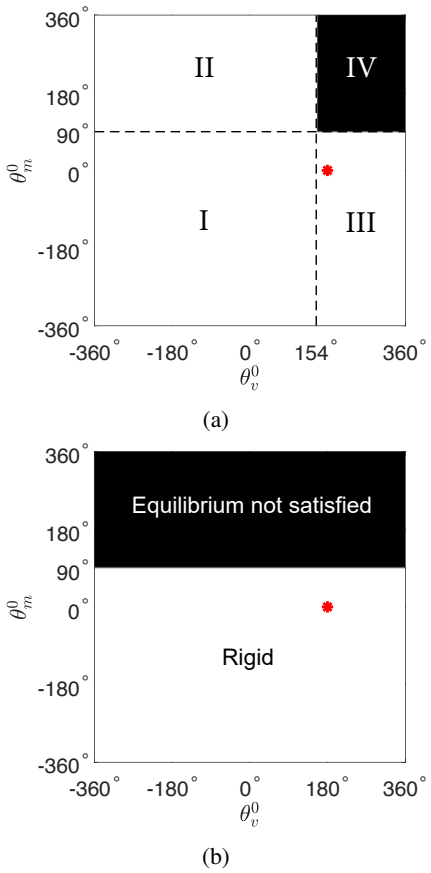

Fig. 6: Design space of the 24-DOF morphing surface. (a) Spherical configuration. Region I satisfies rigidity for any stiffness ratio, while region IV violates equilibrium for all stiffness ratios. In region II, rigidity is maintained above some value of k_v/k_m and in region III, rigidity is maintained below some value of k_v/k_m. (b) Flat configuration. The partition holds for all k_v/k_m. The red dot marks the design used for the prototype, $(\theta_v^0, \theta_m^0) = (180^\circ, 0^\circ)$.

4.5 Prototype

This section presents a prototype of the 24-DOF kirigami surface that is rigid in the flat and spherical configurations. Following Section 4.4, both the flat and spherical configurations are rigid if $\theta_v^0 = 180^\circ$, $\theta_m^0 = 0$, $k_v/k_m < 1.33$, and stops restrict all mountain folds to $\boldsymbol{\theta}_m \geq 90^\circ$.

To fabricate compliant folds with these properties, lamina emergent torsional (LET) joints [15] were designed. LET joints connect two plates with a series of slender cutout beams. The beams twist as the plates rotate with respect to each other, which imparts stiffness to the fold. A specific stiffness value can be obtained from the dimensions of the beams, and several values of the rest angles can be achieved by cutting the plates as separate components and attaching them at an angle.

To achieve a compliant valley fold with a rest angle of 180°, a LET joint was created using two separate plates, as shown in Figure 7a. The plates were connected with screws to form a compliant fold with a fully closed rest angle, as shown in Figure 7b. To achieve a compliant mountain fold with a rest angle of 0°, the LET joint was cut from a single flat sheet. Figure 8a shows a component consisting of a square tile attached to four plates with a zero rest angle LET joint. A clip was added to the mountain folds to restrict the angle to greater than 90°. The clip was cut from a 0.51 mm thick stainless steel sheet and bent to an angle that, when attached to the mountain fold, restricted its angle to greater than 90°. A photo of one mountain fold with the clip applied is shown in Figure 8b. Both the mountain and valley folds were cut from 0.635 mm thick spring steel by waterjet.

There is no specifically required valley to mountain fold stiffness ratio. For any value less than 1.33, both configurations satisfy the rigidity conditions. An approximation of the torsional stiffness of a LET joint can be made using a simple beam torsion model [15]. Using this approximation, the stiffness of the valley and mountain folds are estimated to be 59.9 and 72.9 N mm/rad, respectively. The corresponding stiffness ratio of 0.82 falls within the required range for rigidity in both configurations with margin for error.

Using the LET mountain and valley folds as the primary building blocks, a full prototype of the surface was assembled. The scale of the structure was set by the tile side length of 6.75 cm. The radius of the corresponding target spherical surface is 19.6 cm. Since the pattern is non-developable it must be fabricated as an assembly of separate components.

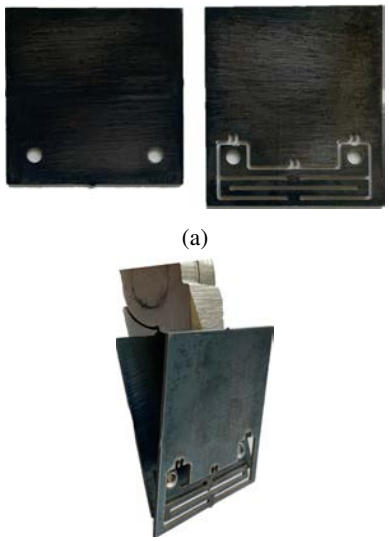

(a)

(b)

Fig. 7: Photos of the compliant valley fold design. (a) Initially cut as two separate plates. (b) The plates were attached with screws and held partially open. This creates a compliant fold with rest angle 180°.

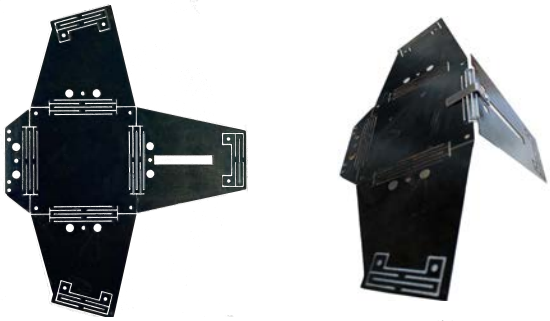

(a) (b)

Fig. 8: Photos of compliant mountain fold design. (a) Initially cut from a flat sheet. (b) Partially assembled with 90° clip attached to one mountain fold. The mountain fold has rest angle 0 and is restricted to greater than 90° by the clip.

Fabrication and assembly of the prototype was a two step process. The inner 3-by-3 grid of tiles and the outer tiles were assembled separately, then joined to complete the structure. Cut patterns for the inner and outer tiles are shown in Figure 9.

The inner 3-by-3 grid of tiles was cut as 9 individual components. Each component consists of a square tile and the surrounding four facets. The edges of the square tile are compliant mountain folds. The first step in the assembly process was to attach the clip to each mountain fold, as shown in Figure 8b where the clip has been attached to one mountain fold. Once the mountain folds were held to 90° by the clips, adjacent tiles were connected. Connections between adjacent tiles are compliant valley folds following the design of Figure 7.

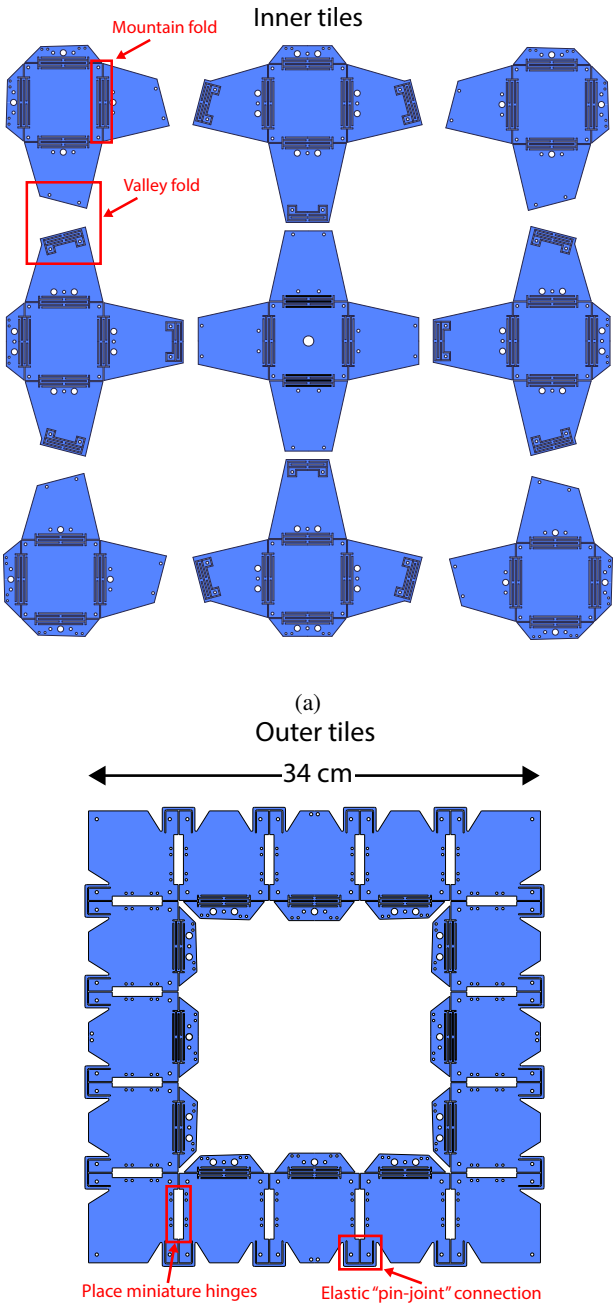

Fig. 9: Prototype cut pattern, consisting of (a) inner tiles and (b) outer tiles. To assemble, 90° clips were attached to each mountain fold. Then, valley folds of the inner tiles were attached with screws. The inner tiles were placed inside the outer tiles and the connecting valley folds were fastened.

The outer loop of 16 tiles was cut from a single sheet. In the fold pattern, the corners of adjacent squares lying on the outer perimeter are joined. To emulate the kinematics of a pin-joint connection, a beam attaches the corners of the outer squares as shown in Figure 10.

The folds connecting the outer tiles are too small to use LET joints. Thickness of the plate and kerf of the waterjet

are limiting factors on the minimum size of the LET joints. Instead, miniature hinges (8 by 10 mm when flat) were used for the outer folds, as shown in Figure 10. While these are not compliant hinges, the compliance of the folds on the inner tiles is sufficient to achieve rigidity.

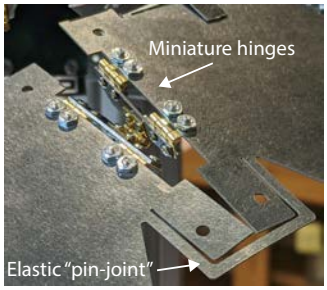

Fig. 10: Design of the folds connecting the outer tiles. Miniature hinges were used instead of LET hinges due to the small geometric features. An elastic beam connects the outer corners of adjacent squares to imitate pin-joint kinematics.

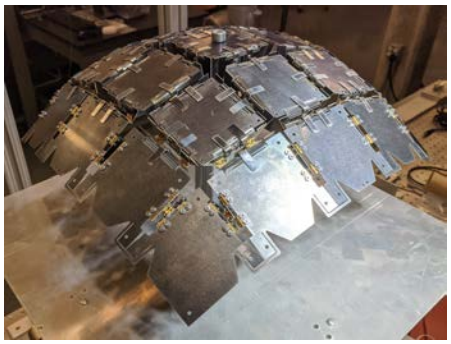

(a)

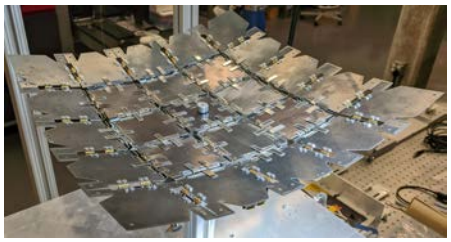

(b)

Fig. 11: Prototype of the 24-DOF morphing surface. (a) Spherical configuration. (b) Flat configuration.

Finally, the assembled inner tiles were attached to the outer tiles. Miniature hinges are also used for the valley folds connecting the inner tiles to the outer tiles due the small size of the fold. A photo of the complete prototype is shown in Figure 11. The structure was mounted by clamping the center tile to an external support underneath the structure.

As expected, the structure is immobilized in the spherical and flat configurations. Actuation between the two configurations is straightforward, despite the 24-DOF kinematics. For example, upward forces on the four corners transforms the structure from spherical to flat while downward forces on the corners transforms flat to spherical.

It was observed that the physical prototype does not exactly achieve the desired flat and spherical shapes. In particular, the flat configuration is not perfectly planar. This is due to elastic compliance of the physical components that were modeled with perfect plate-hinge kinematics. LET joints are known to have unwanted kinematics beyond those of a perfect rotational hinge, such as relative torsion and tension between the plates connected by the joint [22]. Furthermore, the 90° degree clips have some flexibility and do not restrict the mountain folds exactly to the desired range. Despite these undesired sources of compliance, the prototype qualitatively produced the desired behavior.

To demonstrate a practical application of this work, the prototype was outfitted with antenna elements above each tile to create a phased-array antenna. The prototype with antennas mounted is shown in Figure 12. Details regarding the architecture and performance of the antenna from the electrical engineering perspective are presented in [16].

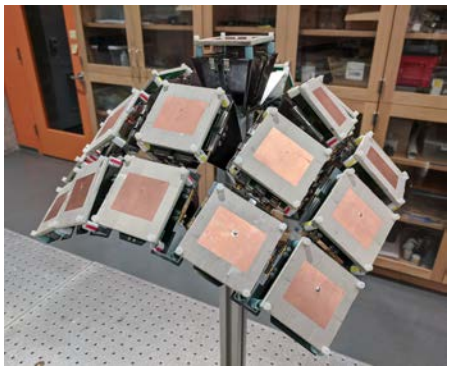

(a)

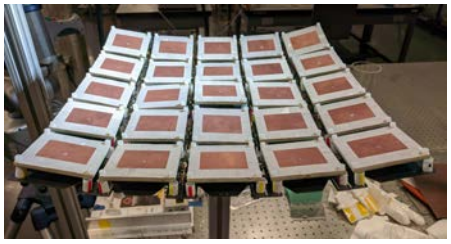

(b)

Fig. 12: Prototype structure with phased array antenna tiles. (a) Spherical configuration. (b) Flat configuration.

5 Conclusion

This work has presented the concept of multi-configuration rigidity, where multiple configurations are made rigid by unilateral contact. Two example structures have been studied: a single-DOF four bar linkage and a 24-DOF kirigami surface. The advantages of multi-configuration rigidity have been highlighted, when compared to multi-stability. First, multi-configuration rigidity is advantageous because each configuration can rigidly resist perturbation forces up to a finite magnitude. Second, the design

space of spring parameters leading to rigidity is larger, which is especially useful for physical implementation. A prototype of the 24-DOF surface was built, with the flat and spherical configurations designed to be rigid using angle stops. The prototype was outfitted with antenna tiles to create a functional phased array antenna, demonstrating a practical application of this structural design concept.

This study serves as an introduction to the concept of multi-configuration rigidity, opening the door to several directions of further research. More general studies could optimize unilateral constraint placement and explore other types of unilateral constraints, such as cables and no-tension struts. Additionally, springs could be designed to maximize the perturbation forces that can be rigidly resisted in each configuration. Ultimately, multi-configuration rigidity could enable practical applications of many-DOF structures and advance applications of reconfigurable structures that require load-bearing capabilities.

Acknowledgements

This work was carried out as part of the AFOSR MURI project Universal Electromagnetic Surface: Exploiting active electronics and active origami to generate a programmable electromagnetic response, supported by the Air Force Office of Scientific Research under award number FA9550-18-1-0566 directed by Dr. Ken Goretta. Discussions with Robert Lang regarding geometry synthesis and with Ali Hajimiri and D. Elliott Williams on the antenna part of the prototype in Section 4.5 are specifically acknowledged.

References

[1] Resch, R. D., 1973. "The topological design of sculptural and architectural systems". In Proceedings of the June 4-8, 1973, national computer conference and exposition, pp. 643–650.

[2] Nassar, H., Lebée, A., and Monasse, L., 2017. "Curvature, metric and parametrization of origami tessellations: theory and application to the eggbox pattern". *Proceedings of the Royal Society A: Mathematical, Physical and Engineering Sciences,* **473**(2197).

[3] Balkcom, D. J., and Mason, M. T., 2008. "Robotic origami folding". *The International Journal of Robotics Research,* **27**(5), pp. 613–627.

[4] Magliozzi, L., Micheletti, A., Pizzigoni, A., and Ruscica, G., 2017. "On the design of origami structures with a continuum of equilibrium shapes". *Composites Part B: Engineering,* **115**, pp. 144–150.

[5] Jape, S., Garza, M., Ruff, J., Espinal, F., Sessions, D., Huff, G., Lagoudas, D. C., Hernandez, E. A. P., and Hartl, D. J., 2020. "Self-foldable origami reflector antenna enabled by shape memory polymer actuation". *Smart Materials and Structures,* **29**(11), p. 115011.

[6] Zhu, Y., Birla, M., Oldham, K. R., and Filipov, E. T., 2020. "Elastically and plastically foldable electrothermal micro-origami for controllable and rapid shape morphing". *Advanced Functional Materials,* **30**(40).

[7] Hawkes, E., An, B., Benbernou, N. M., Tanaka, H., Kim, S., Demaine, E. D., Rus, D., and Wood, R. J., 2010. "Programmable matter by folding". *Proceedings of the National Academy of Sciences,* **107**(28), pp. 12441–12445.

[8] Na, J.-H., Evans, A. A., Bae, J., Chiappelli, M. C., Santangelo, C. D., Lang, R. J., Hull, T. C., and Hayward, R. C., 2015. "Programming reversibly self-folding origami with micropatterned photo-crosslinkable polymer trilayers". *Advanced Materials,* **27**(1), pp. 79–85.

[9] Li, Y., and Pellegrino, S., 2020. "A theory for the design of multi-stable morphing structures". *Journal of the Mechanics and Physics of Solids,* **136**, p. 103772.

[10] Coulais, C., Sabbadini, A., Vink, F., and van Hecke, M., 2018. "Multi-step self-guided pathways for shape-changing metamaterials". *Nature,* **561**(7724), pp. 512–515.

[11] Zareei, A., Deng, B., and Bertoldi, K., 2020. "Harnessing transition waves to realize deployable structures". *Proceedings of the National Academy of Sciences,* **117**(8), pp. 4015–4020.

[12] Ghosh, R., Ebrahimi, H., and Vaziri, A., 2014. "Contact kinematics of biomimetic scales". *Applied Physics Letters,* **105**(23), p. 233701.

[13] Salisbury, J. K., and Roth, B., 1983. "Kinematic and force analysis of articulated mechanical hands".

[14] Bicchi, A., 1995. "On the closure properties of robotic grasping". *The International Journal of Robotics Research,* **14**(4), pp. 319–334.

[15] Jacobsen, J. O., Chen, G., Howell, L. L., and Magleby, S. P., 2009. "Lamina emergent torsional (let) joint". *Mechanism and Machine Theory,* **44**(11), pp. 2098–2109.

[16] Williams, D. E., Dorn, C., Pellegrino, S., and Hajimiri, A., 2021. "Origami-inspired shape-changing phased array". In 2020 50th European Microwave Conference (EuMC), IEEE, pp. 344–347.

[17] Trinkle, J. C., 1992. "On the stability and instantaneous velocity of grasped frictionless objects". *IEEE Transactions on Robotics and Automation,* **8**(5), pp. 560–572.

[18] McCarthy, J. M., and Soh, G. S., 2010. *Geometric design of linkages*, Vol. 11. Springer Science & Business Media.

[19] Bazaraa, M. S., Sherali, H. D., and Shetty, C. M., 2013. *Nonlinear programming: theory and algorithms*. John Wiley & Sons.

[20] Li, Y., Chandra, A., Dorn, C. J., and Lang, R. J., 2020. "Reconfigurable surfaces employing linear-rotational and bistable-translational (lrbt) joints". *International Journal of Solids and Structures,* **207**, pp. 22–41.

[21] Schenk, M., and Guest, S. D., 2011. "Origami folding: A structural engineering approach". *Origami,* **5**, pp. 291–304.

[22] Delimont, I. L., Magleby, S. P., and Howell, L. L., 2015. "Evaluating compliant hinge geometries for origami-inspired mechanisms". *Journal of Mechanisms and Robotics,* **7**(1).

